Trends and ENSO-related variability in Atlantic tropical cyclone intensity and intensification

Michael K. Tippett[a] and Suzana J. Camargo[b]

[a] *Department of Applied Physics and Applied Mathematics, Columbia University, New York, New York*

[b] *Columbia Climate School, Columbia University, New York, New York*

Corresponding author: M. K. Tippett, mkt14@columbia.edu

ABSTRACT: This study examined trends and ENSO-related variability in Atlantic tropical cyclone intensity, focusing on 24-h intensification, lifetime maximum intensity (LMI), and rapid intensification (RI) in best-track data during the period 1982–2024. Previous studies considered trends and ENSO influences separately, reporting upward trends in intensity and more cases of RI during La Niña conditions. Here we extended and built upon prior work by including data through 2024, assessing the impact of ENSO on LMI and 24-h intensification, and analyzing a new storm metric called lifetime maximum 24-h intensification (LM24I). The statistical methods employed here improve upon previous ones by better assessing uncertainty and statistical significance, simultaneously estimating trends and ENSO-related variability, and addressing problems arising from the 5-kt discretization of best-track intensity data. Quantile and logistic regression were employed extensively. The main findings include the following: Prior estimates of intensification trends were overconfident, and including recent data reduces prior estimates of trends in intensification, RI frequency, and LMI. The distribution of LM24I shows significant upward trends of 3–5 kt per decade in its top quantiles and broad increases of 2–5 kt per degree of Niño-3.4 cooling. During La Niña conditions, the frequencies of RI events and RI storms increase, and the distributions of 24-h intensification and LMI show previously unreported broad and significant increases. Directions for future research include applying the same approaches to other intensity metrics, basins, and model output, and leveraging ENSO predictability for seasonal intensity prediction.

SIGNIFICANCE STATEMENT: This study examined how the intensity (wind speed) of tropical cyclones in the Atlantic has changed over time and how it varies with El Niño and La Niña. In terms of trends, the most intense storms are becoming stronger and the most extreme rapid intensification is becoming more frequent. During La Niña conditions, intensification rates are higher and hurricanes are stronger. Use of better statistical techniques and additional data resulted in reduced upward trends compared to prior estimates and a more comprehensive picture of the impacts of El Niño and La Niña on Atlantic tropical cyclone intensity.

1. Introduction

Tropical cyclones are among the most destructive natural disasters, causing damage and loss of life through storm surge, high winds, and heavy rainfall. The hazard posed by tropical cyclones can be characterized by a range of features, including their track, size, translation speed, and intensity. Of these characteristics, maximum sustained wind speed (intensity) receives particular attention and is a commonly used metric for classifying storm severity, though other intensity measures (e.g., surface pressure; Klotzbach et al. 2020) and factors (e.g., storm size; Zhai and Jiang 2014) may better determine the impact of a particular storm. This study focuses on two aspects of Atlantic tropical cyclone intensity: trends and ENSO-related variability. Observed long-term trends in tropical cyclone intensity and intensification provide information for what to expect in a changing climate as well as validation for models and theory (Knutson et al. 2019, 2020; Camargo et al. 2023). ENSO-related variability in tropical cyclone behavior is especially relevant on interannual timescales since ENSO is the primary source of seasonal predictability.

Upward tropical cyclone intensity trends are expected in a warming climate on the basis of potential intensity theory (e.g., Sobel et al. 2016) and high-resolution models (e.g., Knutson et al. 2010). Kossin et al. (2013, their Figs. 5 and 10) found positive trends in quantiles above the median of lifetime maximum intensity (LMI) for Atlantic storms that reached hurricane strength in Advanced Dvorak Technique Hurricane Satellite (ADT-HURSAT) data and in best-track data over the period 1982–2009. Over the same 1982–2009 period, Bhatia et al. (2019, their Fig. 2c) found statistically significant positive trends in annual quantiles of Atlantic basin 24-h intensification above the 0.6 quantile (3 kt decade^{-1} in the 0.95 quantile) and negative significant trends in quantiles below the 0.45 quantile using International Best Track Archive for Climate Stewardship

(IBTrACS) data. Significant trends in the quantiles of 24-h intensification from ADT-HURSAT data were limited to the most extreme quantiles — positive in the 0.9 and 0.95 quantile (4 kt decade^{-1}), and negative in the 0.05 and 0.1 quantiles (Bhatia et al. 2019, their Fig. 2d). Bhatia et al. (2019, their Fig. 3b) also found a significant upward trend in the frequency of rapid intensification (RI; 24-h intensification greater than 30 kt) in the Atlantic basin. Based on bias-corrected model simulations, they concluded "natural variability cannot explain the magnitude of the observed upward trend." Balaguru et al. (2018) examined Atlantic storm intensification at sub-basin resolutions over the period 1986–2015 and found a significant upward trend (3.8 kt decade^{-1}) in the 0.95 annual quantile of 24-h intensification east of 60°W and no significant trend in intensification to the west. They speculated that the upward intensification trend in the eastern region was due to the Atlantic Multidecadal Oscillation (AMO) transitioning from a negative to a positive phase over the same period. In another regional analysis, Balaguru et al. (2022) found statistically significant increases in the average 24-h intensification of storms near the U.S. Atlantic coast for the period 1979–2018, but not for storms near the Gulf coast, though RI frequency increased in both regions.

ENSO influences Atlantic tropical cyclones through changes in vertical shear and stability that make conditions less favorable for storm formation and intensification during El Niño and more favorable during La Niña conditions (Gray 1984; Bove et al. 1998; Tang and Neelin 2004; Klotzbach 2011). Jagger and Elsner (2009) examined the influence on ENSO on maxima of near-coastal tropical cyclone intensity interpolated from HURDAT and found that the average and 0.5–0.9 quantiles increased as the Southern Oscillation Index increased toward La Niña-like conditions. Klotzbach (2012, their Fig. 2) stratified RI events by ENSO state during the period 1974–2010 and found that nearly three times as many RI events occurred in La Niña years as in El Niño years for a range of RI thresholds (intensification of at least 25, 30, 35, or 40 kt in a 24-h storm period). Klotzbach (2012, their Table 2) also found that the frequency of RI storms (storms that undergo RI at some point during their lifetime) was higher during La Niña years than during El Niño years. Wang et al. (2017, their Table 1) found that over the period 1950–2104 the number of North Atlantic RI events (30 kt threshold) was significantly correlated ($r = -0.45$) with the June–November average Niño-3.4 index. Klotzbach et al. (2022, their table S4) found a negative correlation (-0.41) between 50-kt RI event numbers and the ENSO Longitude Index (ELI; Williams and Patricola 2018) over the recent period 1990–2021.

Questions remain regarding trends and ENSO-related variability in Atlantic tropical cyclone intensification. For instance, Klotzbach (2012) left open the question of whether the higher number of RI events during La Niña years was due to increased likelihood of RI during La Niña years or due to simply more storms and more opportunities for RI (annual numbers of storms and RI events are significantly correlated; Wang et al. 2017, their Table 4). Although RI is known to be related to LMI (e.g., Lee et al. 2016), to date, the relation of ENSO with LMI has not been examined. Previous trend results may be specific to the period examined. For instance, although Bhatia et al. (2019) found trends in RI frequency, Wang et al. (2017) considered the longer period 1950–2014 and noted no long-term trend in RI numbers. Likewise Klotzbach et al. (2022, their table S2) found no significant trends in Atlantic RI events (30 kt and 50 kt thresholds) over the recent period 1990–2021. Whether trends are limited to a past period or whether they extend to present is an important consideration in deciding if trend information might be used to anticipate future conditions, though decadal variability such as the Atlantic Multidecadal Oscillation with its phase transition in the mid-1990s (Goldenberg et al. 2001) complicates such interpretations.

There are also methodological questions. For instance, accurately assessing statistical significance is critical when the signals in question are modest. Therefore, an issue of interest is whether the ad hoc procedure in Bhatia et al. (2019, 2022) that added random noise to the observations to mimic observational error accurately captured the uncertainty of trend estimates. Some trend analysis first computed annual quantiles for each year and then fit trends in those annual quantiles by ordinary least squares (OLS) regression (e.g., Balaguru et al. 2018; Bhatia et al. 2019). Other analysis used quantile regression which pools all the data in the fitting procedure and computes trends via least asymmetric absolute loss (e.g., Jagger and Elsner 2009; Elsner and Jagger 2013; Kossin et al. 2013). To date the theoretical or practical differences between these approaches have not been investigated in the context of tropical cyclone trends. A similar issue arises in the analysis of frequency trends (e.g., frequency of RI events or frequency of RI storms). One approach is to compute the annual proportion for each year first and then to compute their trends by OLS regression (e.g., Bhatia et al. 2019). On the other hand, logistic regression, which is commonly used in RI forecast applications (e.g., Knaff et al. 2018), is specifically designed for analysis of frequencies and has the advantage of taking account of all the event data in the fitting process. As with quantile regression, the theoretical or practical differences between these approaches have not

been examined in the context of RI trends. Previous analysis has considered trends and ENSO separately. Accounting for ENSO variability might reduce the uncertainty in trend estimates. A final methodological point is that best-track intensity data are recorded in 5 kt increments. Statistical methods that assume continuous random variables tend to perform poorly with discrete data, which is an issue whose implications have not been investigated in the context of tropical cyclone intensification.

In this paper we have addressed several of the questions and gaps identified above. With regard to ENSO-related variability, we extended the studies of Klotzbach (2012) and Wang et al. (2017) which found more RI events during cool ENSO conditions, to consider the question of whether such increases are simply due to an increase in tropical storm activity (more 24-h storm periods) during cool ENSO conditions or whether RI events are inherently more likely. We also examined the influence of ENSO state on 24-h intensification, beyond just RI, and on LMI. We explored whether trends may be specific to past periods by (i) using data through 2024 and (ii) repeating some analysis with start years of 1950, 1960, 1970, and 1982. The 1982 start year was chosen to match the trend studies of Kossin et al. (2013) and Bhatia et al. (2019). We used regression methods that permit treating trends and ENSO-related variability simultaneously. We focused on two methodological issues: whether adding random noise to the observations results in accurate assessments of trend uncertainty and statistical significance, and how discrete intensity data affect the calculation of quantiles and quantile regression. We also discussed differences between OLS and advanced (quantile and logistic) regression methods and compared results in a few cases.

The paper is organized as follows. Data and methods are described in Section 2, including logistic and quantile regression. The impact of quantized best-track intensity data on statistical analysis is examined in Section 3 along with recommendations on the use of jitter. Trends and ENSO-related variability are reported in Section 4. Results are summarized and directions for future work are provided in Section 5.

2. Data and methods

a. Data

Most of the analysis used the period 1982–2024. For composites, the early period was defined to be 1982–2002 (21 years) and the late period to be 2003–2024 (22 years). For the quantile

regression analysis, we repeated the calculations using as start years: 1950, 1960, and 1970 to see the robustness of the results and their sensitivity to period. An important caveat to start years prior to 1980 is the lack of satellite data during part of the period and its impact on the quality and completeness of the best-track intensity data.

The ENSO state was characterized by the August–October (ASO) Niño-3.4 index, which is the average of sea surface temperature (SST) in the region 170°W–120°W, 5°S–5°N (Barnston et al. 1997). SST data 1950–2024 were taken from ERSSTv5 (Huang et al. 2017). For composites, El Niño (warm) and La Niña (cool) years were defined to be ones whose ASO Niño-3.4 index values were in the upper and lower quartiles, respectively, of the data (Hanley et al. 2003). The thresholds for the period 1982–2024 are +0.54°C for El Niño and -0.63°C for La Niña, expressed as anomalies with respect to the mean over the period. These thresholds resulted in 11 El Niño years: 1982, 1986, 1987, 1991, 1994, 1997, 2002, 2004, 2009, 2015, and 2023 (also classified as ASO El Niño by NOAA's Climate Prediction Center) and 11 La Niña years: 1983, 1988, 1995, 1998, 1999, 2007, 2010, 2011, 2020, 2021, and 2022 (also classified as ASO La Niña by NOAA's Climate Prediction Center).[1] The average difference between warm and cool year values of ASO Niño-3.4 is 2.2°C. Classifications of ENSO phases that select other years because of different Niño-3.4 thresholds or ENSO indices could impact composite analysis results.

Atlantic tropical cyclone data 1950–2024 were taken from the International Best Track Archive for Climate Stewardship (IBTrACS, V04r01; Knapp et al. 2010; Gahtan et al. 2024). Intensity values were taken from the USA_WIND entries. The storm data were filtered to retain entries: at 0, 6, 12, and 18 UTC, during June–November, over ocean (DIST2LAND > 0), and with Saffir-Simpson ratings of "tropical storm" and greater (USA_SSHS ≥ 0). This filtering leaves only 6-hourly snapshots with intensities of 35 kt or greater and US_STATUS labels of tropical storm and hurricane; no disturbances, depressions, subtropical storms or extratropical systems are included. Measures of tropical cyclone intensity and intensification considered were: LMI (lifetime maximum intensity; one value per storm), 24-h intensification (all over-lapping 24-h storm periods), RI events (yes/no per 24-h period), and RI storms (yes/no per storm) using RI thresholds of 20 kt to 40 kt by 5 kt. We also analyzed a new quantity called lifetime maximum 24-h intensification (LM24I; one value per storm) shown in Fig. 1. The minimum and mean lifetime of storms included in LM24I analysis is 1 day and 5.3 days, respectively. LM24I is negative for seven

[1] https://origin.cpc.ncep.noaa.gov/products/analysis_monitoring/ensostuff/ONI_v5.php

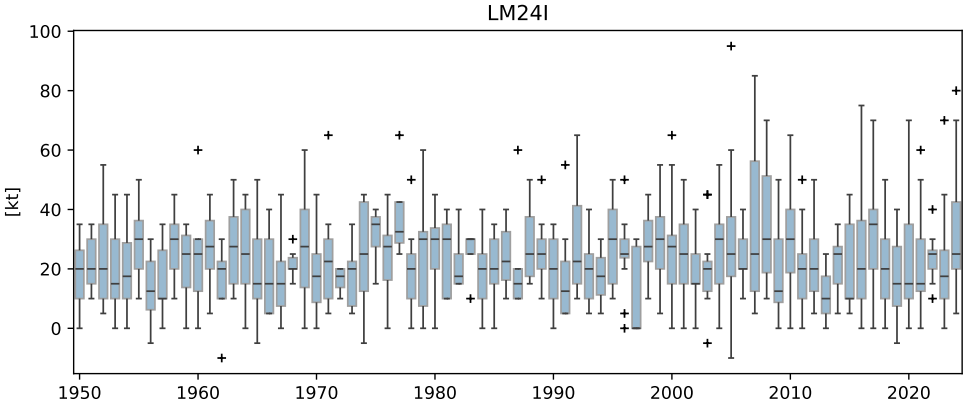

FIG. 1. Boxplots of lifetime maximum 24-h intensification (LM24I) values by year for Atlantic tropical storms and hurricanes. The box covers the interquartile range (IQR) with a line that marks the median. Whiskers extend to the smallest and largest data points within 1.5 times the IQR from the lower and upper quartiles, respectively. Plus signs are values outside this range.

storms (less than 1% of the total). The most recent case was Melissa which evolved in October of 2019 from an extratropical low to a subtropical storm and then to a tropical storm. Melissa (2019) only weakened during its time as a tropical storm, and therefore its LM24I is negative (-5 kt).

In the summary and conclusions, we briefly examine intensification in the ADT-HURSAT data record for the period 1989–2017, which provides satellite-based estimates of tropical cyclone intensity (Kossin et al. 2013, 2020).

b. Methods

1) DISTRIBUTIONS

Data were stratified into early/late periods and warm/cool ENSO years. The statistical significance of differences between samples from early and late periods, as well as from warm and cool ENSO years, was assessed using the two-sample Kolmogorov-Smirnov (KS) test, which is a nonparametric test that addresses the question of whether two sets of samples come from the same probability distribution. The test statistic is

$$\text{KS test statistic} = \max_x |F_1(x) - F_2(x)|$$

where F_1 and F_2 are the empirical cumulative distribution functions of the two samples. Since the empirical cumulative distribution functions vary between zero and one, the KS test is most sensitive to differences near the center and less sensitive in the tails. Distributions were plotted as histograms (bins with width of 5 kt, centered on multiples of five), kernel smoothed probability density functions, and return level plots that use the approximate return period $-1/\log f$ where f is the cumulative frequency (DelSole and Tippett 2022). Return level plots contain the same information as cumulative distribution plots but provide a clearer representation of the behavior of extreme values by replacing small exceedance probabilities with large return periods and using a log scale. Since the KS test is based on the vertical distance between the empirical cumulative distribution functions, it cannot be directly read from plots of probability density functions or return levels.

2) Contingency tables

Differences in occurrence counts (e.g., number of RI events or RI storms) between early/late periods and warm/cool ENSO years were tabulated in 2×2 contingency tables. For example, a 2×2 table for RI events and warm/cool years has the form:

	RI	no-RI
Warm	a	b
Cool	c	d

where a, b, c, and d are the number of cases. The odds ratio is a standard measure of association for 2×2 contingency tables and is used to measure the dependence between two variables, in this example, ENSO state and RI occurrence. The odds of RI during warm and cool conditions are a/b and c/d, respectively. The odds ratio (cool/warm) is cb/ad. Values of the odds ratio greater than one indicate more frequent RI events during cool conditions, and values near one (equal odds) favor deciding no association. Fisher's exact test was used to compute the statistical significance of contingency tables and confidence intervals for the odds ratio.

3) Logistic regression

Logistic regression relates the log odds of an event to a linear function of covariates (predictors variables). Here logistic regression was applied to occurrence of RI events (yes/no per 24-h period),

and RI storms (yes/no per storm), and the covariates were time (in decades) and the Niño-3.4 index. The logistic regression has the form

$$\text{log odds} = \log\left(\frac{p}{1-p}\right) = \beta_0 + \beta_{\text{time}}\,\text{time} + \beta_{\text{Niño-3.4}}\,\text{Niño-3.4}\,,$$

where p is the probability of the event conditional on time and the Niño-3.4 index. Logistic regression is an alternative to computing annual proportions and fitting an OLS regression to those annual values. Advantages of logistic regression include: the resulting proportions are bounded between zero and one; confidence intervals are more accurate; sensitivity to outliers is reduced; the OLS assumption of uniform variance residuals (violated for proportions near zero or one) is avoided; the fitting procedure sees all the data and accounts for different numbers of events per year. To illustrate the last point, consider an intercept-only regression (horizontal line) which computes the climatological frequency of RI events. The logistic regression approach correctly computes the frequency as the number of occurrences divided by the number of RI opportunities. The OLS approach, however, first computes the frequency for each year and then averages those annual frequencies, which gives an incorrect result when the number of RI opportunities varies from year to year.

Logistic regression coefficient values are the log odds change for a unit change in the covariate. The corresponding probability change is a nonlinear function of the odds change, which means that the change from a baseline probability for a unit change in covariate depends on both the logistic regression coefficient and the baseline probability value. To show the nonlinear dependence of the logistic regression probability on its covariates, and we plotted the probability as function of one covariate and held the other covariate fixed to its average value.

4) Quantile regression

Quantile regression models the quantiles of a quantity as a linear function of covariates. Here we applied quantile regression to 24-h intensification, LM24I, and LMI and used as covariates time (in decades) and the Niño-3.4 index. Namely, the conditional quantile Y_τ was modeled as

$$Y_\tau = \beta_{0,\tau} + \beta_{\text{time},\tau}\,\text{time} + \beta_{\text{Niño-3.4},\tau}\,\text{Niño-3.4}\,. \tag{1}$$

The conditional τ-quantile of a quantity Y is the threshold so that $\text{Prob}(Y \leq Y_\tau|\text{time, Niño-3.4}) = \tau$. For instance, the probability level $\tau = 0.5$ corresponds to the conditional median. The quantile regression coefficients were computed separately for each probability level τ by optimizing asymmetric absolute loss (AAL; Koenker and Bassett 1978). Quantile regression is an alternative to computing annual quantiles for each year separately and then fitting an OLS regression to those values. As mentioned in the Introduction, both approaches have been used to analyze trends in tropical cyclone intensity. Like logistic regression, quantile regression has the advantage of using the entire dataset in the fitting process and accounts for differing numbers of events from one year to another. Differing annual numbers of events result in differing levels of uncertainty in the annual quantiles, a factor that is neglected in the subsequent OLS regression, which assumes constant residual variance. Becker and Tippett (2024) compared quantile regression and OLS regression of annual quantiles of December–February daily temperature. In that application, the number of samples each year was fixed (February 29 was excluded), but differences between OLS and quantile regression remained because quantile regression optimizes a different cost function (AAL) and that cost function is a function of all the data, not just annual statistics.

Best-track TC wind speeds are recorded in discrete 5-knot increments. Such quantized data pose challenges for statistical estimation and inference which often assume samples come from a continuous distribution. In the case of quantile regression when data are concentrated in discrete levels, the quantile regression optimization may be unstable or biased, especially for extreme quantiles. Likewise, the KS test, which is used to decide if samples come from different distributions, assumes a continuous cumulative distribution function. Discrete data reduce the test's sensitivity and produce inaccurate p-values. Adding small random noise, or *jitter*, fills in "gaps" where there are no values and results in data with an approximately continuous distribution which better matches the assumptions underlying many parametric and nonparametric statistical methods. The issue of jitter has been discussed in the statistics literature in the context of count data (Machado and Silva 2005). Tippett et al. (2016) used jitter in the analysis of tornado counts. Here we added jitter to the intensity data by adding random numbers uniformly distributed on the interval ±2.5 kt, which matches the 5 kt quantization. Regression coefficients, confidence intervals, and p-values were averaged over 100 realizations of the jitter. Since this issue does not seem to have been addressed

in the tropical cyclone literature, we examine the impact of jittering on quantile estimates and quantile regression in Section 3.

3. Quantization and jitter

When dealing with discrete data, the statistics literature often suggests adding random noise (jitter) whose support (values with non-zero probability) fill in the gaps (Pearson 1950). Jitter that is uniformly distributed on the interval ±2.5 kt accomplishes this for best-track intensity data. However, other levels of jitter have been used with tropical cyclone intensity data. Bhatia et al. (2019) added jitter uniformly distributed on the interval $\pm 2\sqrt{50}$ kt to intensity change values. Kossin et al. (2013) added jitter uniformly distributed on the interval ±1.94 kt (±1 m/s) to LMI values.

a. Computing quantiles

To see the impact of these jitter choices on quantile estimates, we generated synthetic normally distributed data with the same sample size (7682), mean (4), and standard deviation (17) as the 1982–2024 24-h intensification data. We used synthetic data so that the population values of the quantiles are known. We then computed the sample quantiles of the synthetic data and their error compared to the population quantiles. The magnitude of sample quantile errors was less than 0.2 kt (blue dots in Fig. 2a). Repeating the quantile calculation with the same data rounded to the nearest 5 kt (quantized) introduced errors in the quantile estimates which exceed 2 kt (orange dots in Fig. 2a) and are substantially larger than those from sampling variability. Adding jitter uniformly distributed on the interval $\pm 2\sqrt{50}$ kt to the quantized data introduced a systematic bias in the quantiles which is negative for quantiles below the median, positive for quantiles above the median, and larger for more extreme quantiles (Fig. 2b). The reason for this bias is that the variance of a sum of independent random variables is the sum of their variances. Therefore while adding mean-zero random values leaves the mean unchanged, the variance is increased, which shifts high quantiles upward and low quantiles downward, as observed here. Too large jitter biases quantile estimates. Adding jitter uniformly distributed on the interval ±1.94 kt reduced the quantile errors compared to those of the quantized data, though they remain noticeable. Too small jitter fails to fill in gaps in discrete data ($1.94 < 2.5$). Adding jitter uniformly distributed on the interval ±2.5 kt

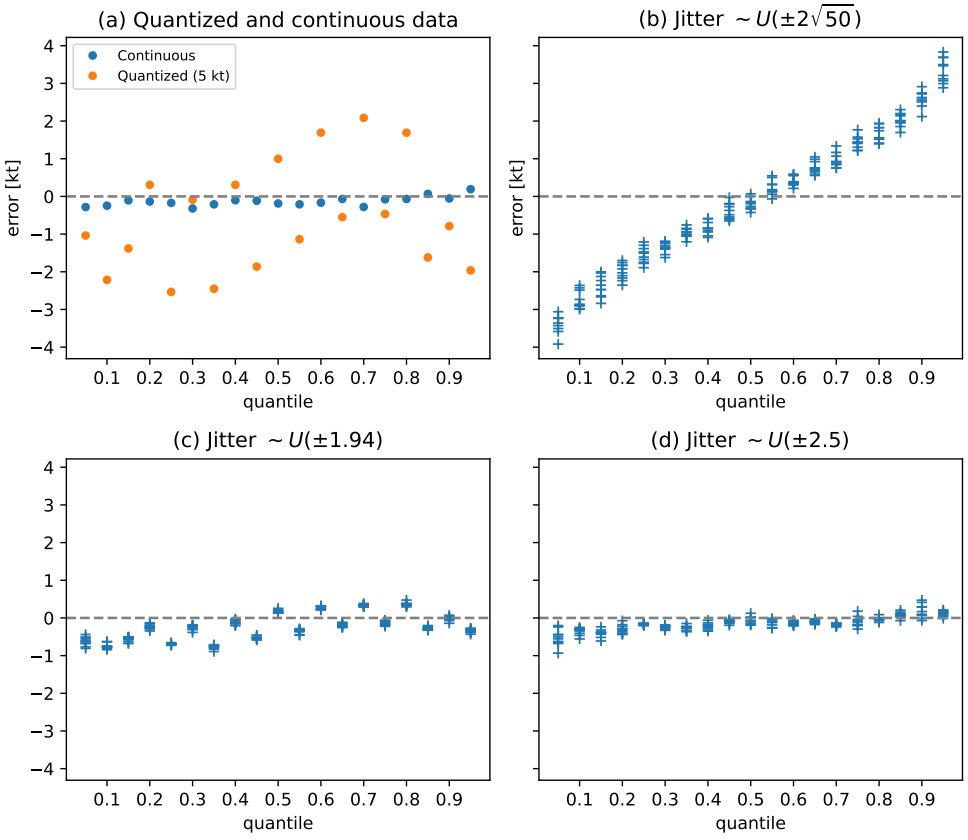

FIG. 2. Errors of quantile estimates at probability levels 0.05–0.95 by 0.1 for (a) synthetic continuous data (blue) and the same data quantized to the nearest 5 kt (orange), (b) the quantized data with jitter (random noise) uniformly distributed on $\pm 2\sqrt{50}$ kt added, (c) the quantized data with jitter uniformly distributed on ±1.94 kt added, and (d) the quantized data with jitter uniformly distributed on ±2.5 added. Panels b, c, and d show the quantile estimate errors for 10 realizations of the jitter.

matches the gaps in the discrete data and resulted in errors that are comparable on average to those due to sampling variability (Fig. 2d). The results of the synthetic data experiment support the use of jitter uniformly distributed on the interval ±2.5 kt when estimating quantiles of intensity data.

b. Quantile regression

A problem when applying quantile regression to discrete data is that the conditional quantile (see Eq. 1) is a discontinuous function of its covariates, i.e., it changes from one discrete value to another. To illustrate the consequences of this issue, we applied quantile regression to synthetic data that is the same size as the 1982–2024 24-h intensification data. The synthetic data were

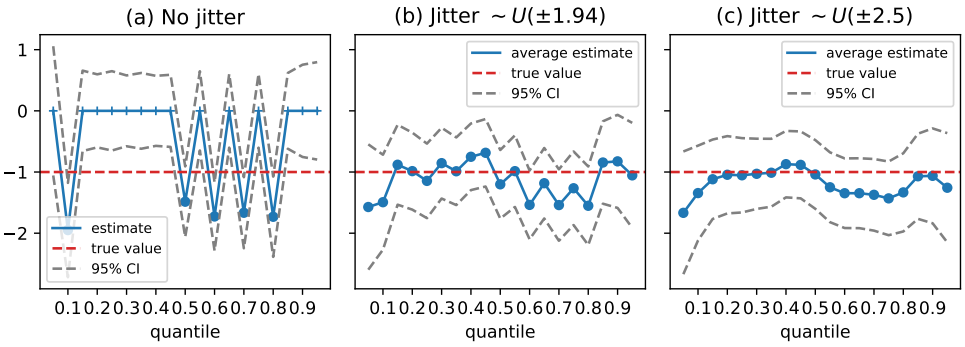

FIG. 3. Quantile regression coefficient estimates (blue lines) from synthetic data (a) without jitter, (b) with jitter uniformly distributed on the interval ±1.94 kt, and (c) with jitter uniformly distributed on the interval ±2.5 kt. The true quantile regression coefficient value is −1 (red dashed line). Dashed gray lines are 95% confidence intervals. Solid blue circles indicate statistical significance at the 5% level.

generated according to

$$y = -\text{Niño-3.4} + \text{noise},$$

where the noise was normally distributed with mean zero and standard deviation 17, and the Niño-3.4 values were the observed ones. By construction, the population quantiles shift by minus one for each one degree increase of Niño-3.4. The synthetic data were then rounded to the nearest multiple of 5 and fit by quantile regression. Without jitter, the quantile regression coefficient estimates show sawtooth behavior and are overly variable (Fig. 3a). The confidence intervals fail to include the true value. After adding jitter that is uniformly distributed on the interval ±1.94 kt to the data, the quantile regression coefficient estimates are closer to their true values but noticeably variable from one probability level to the next, though the confidence intervals include the true value (Fig. 3b). After adding jitter that is uniformly distributed on the interval ±2.5 kt to the data, the quantile regression coefficient estimates are smoother and relatively close to their true values (Fig. 3c). These results support adding jitter that is uniformly distributed on the interval ±2.5 kt when applying quantile regression to intensity data.

c. Uncertainty quantification

To quantify the uncertainty of computed trends, Bhatia et al. (2019) added jitter that was uniformly distributed on the interval $\pm 2\sqrt{50}$ kt to each intensity change value, computed the trend in annual

quantiles by OLS regression, repeated this process 1000 times, reported the average trend, and considered the 5th and 95th percentiles of the 1000 trends as a 90% confidence interval for the trend. The size of the jitter was chosen based on the typical error of intensity observations. However, the typical purpose of adding jitter, as discussed above, is to address quantization effects rather than simulating observation error or quantifying uncertainty. Since observation error is only one source of trend uncertainty, the procedure fails to provide a complete quantification of uncertainty. For instance, in the case of no error or negligible measurement error, the procedure would result in trend estimates with no uncertainty, which is clearly incorrect. Accounting only for observation error underestimates trend uncertainty. Bootstrapping of residuals is a common method of quantifying the uncertainty of regression coefficients. In this method, residuals of a regression are randomly added to the data, and the regression refit, which is similar in spirit to the Bhatia et al. (2019) procedure. However, observational error does not determine the magnitude of regression residuals. For instance, in the case of no relation between predictors and the predictand y, the variance of the residuals is approximately the variance of y, which is larger than the observation error variance for reliable observations (noise less than signal). In general, the variance of the residuals is approximately the fraction of unexplained variance $(1 - r^2)$ times the climatological variance of y.

To see the extent to which the procedure of Bhatia et al. (2019) underestimates the uncertainty of trends, we examined the annual 0.9 and 0.95 quantiles of 24-h intensification data over the period 1950–2024 (Fig. 4a, b). Following the procedure of Bhatia et al. (2019, their Fig. 2c), we computed trends of 0.19 kt yr^{-1} and 0.28 kt yr^{-1} over the period 1982–2009 with 90% interval of [0.095, 0.28] kt yr^{-1} and [0.18, 0.39] kt yr^{-1}, respectively, for the trends of the 0.9 and 0.95 quantile, which visually matches their results. They deemed the trends to be statistically significant at the 10% level since the intervals did not include zero. However, 90% confidence intervals for the 0.9 quantile trends from OLS, bootstrap pairs, and bootstrap residuals (1000 samples) are [-0.04, 0.4], [-0.051, 0.45], and [-0.022, 0.4] kt yr^{-1}, respectively. These intervals are all larger than the Bhatia et al. (2019) interval by more than a factor of two, and all include zero, which means that the trend is statistically insignificant at the 10% level (OLS p-value = 0.17). The 90% confidence intervals for the 0.95 quantile trends from OLS, bootstrap pairs, and bootstrap residuals (1000 samples) are [0.015, 0.58], [0.0034, 0.6], and [0.023, 0.57] kt yr^{-1}, which are larger than the jitter-based ones by nearly a factor of three. Similar considerations apply to the positive trend in RI frequency reported

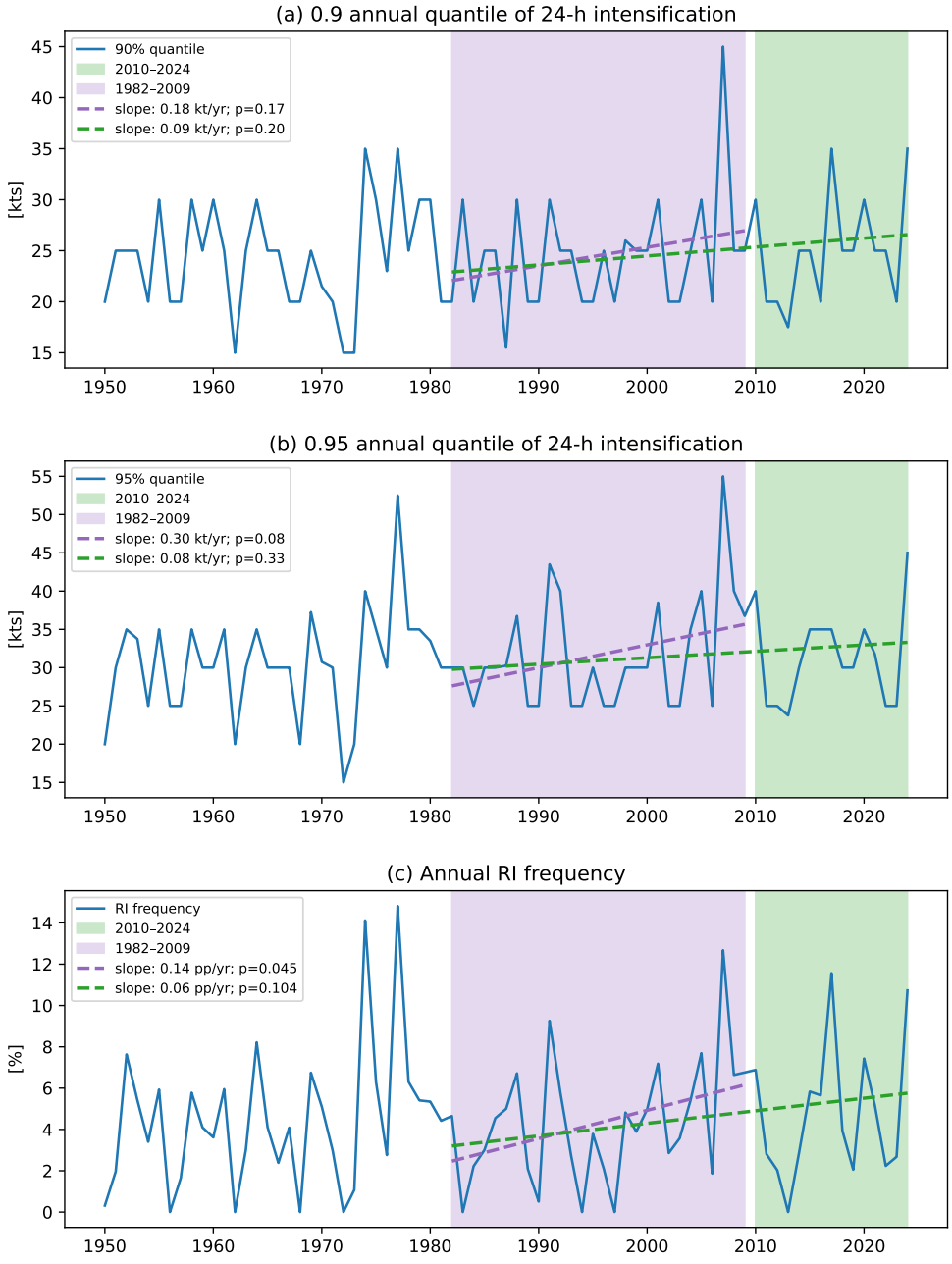

FIG. 4. Time series of (a) 0.9, (b) 0.95 annual quantiles of Atlantic 24-h intensification, and (c) annual Atlantic RI frequency 1950–2024. Values during the periods 1982–2009 and 1982–2024 are fit to linear trends by OLS regression and plotted (dotted lines). OLS regression trends and p-values are shown in the legend.

by Bhatia et al. (2019). We found the same slope of 0.14 percentage points (pp) yr^{-1} over the period 1982–2009 (Fig. 4c) but the OLS 90% confidence interval of [0.026, 0.25] pp yr^{-1} is wider

by more than a factor of two than the interval [0.1, 0.18] pp yr^{-1} reported by Bhatia et al. (2019). Adding jitter to simulate observation error fails to represent regression coefficient uncertainty.

Another point is that examination of the 24-intensification and RI frequency timeseries suggests that the trends may be specific to the choice of period. All three timeseries have higher values prior to the 1982–2009 period, modest values in the 1980s, and an unusually high value in 2007 (strong La Niña). When the analysis period was extended to 2024, the 0.9 and 0.95 annual quantile trends dropped to 0.09 kt yr^{-1} and 0.08 kt yr^{-1} with OLS p-values of 0.20 and 0.33, respectively. Likewise, when the analysis period was extended to 2024, the RI frequency trend dropped to 0.06 pp yr^{-1} and was not statistically significant (p-value = 0.104).

We will see in in Section 4 that quantile regression (as opposed to OLS regression with annual quantiles) finds significant upward intensification trends in the 0.9 and 0.95 quantiles over the period 1982–2024. Similarly we will see in Section 4 that logistic regression (as opposed to OLS regression of annual proportions) with time and Niño-3.4 as covariates finds significant upward RI (30 kt threshold) frequency trends over the period 1982–2024. We discuss how year-to-year variations in sample size is one potential reason for these different results in Section 5.

4. Trends and ENSO-related variability

a. 24-h intensification

We first examined trends and ENSO-related variability in Atlantic 24-h intensification values. Differences in the distribution of 24-h intensification values between early and late periods are statistically insignificant, and the probability density functions are visually indistinguishable (Fig. 5a). The return level curves reveal that late period intensification rates greater than 25 kt are shifted toward shorter return periods, which means they occur more frequently (Fig. 5c). Differences in the distribution of Atlantic 24-h intensification values between warm and cool ENSO years are statistically significant, and the kernel smoothed density functions show a modest but consistent shift rightward for positive 24-h intensification values during cool years (Fig. 5b). This shift in cool ENSO years results in a reduction of return periods for positive 24-h intensification values, and the return period reduction is larger at higher values (Fig. 5d). Quantile regression of 24-h intensification with time and Niño-3.4 as covariates shows that significant trends are limited to the 0.9 and 0.95 quantiles (0.6 and 1.5 kt $decade^{-1}$, respectively) over the 1982–2024 period. Negative

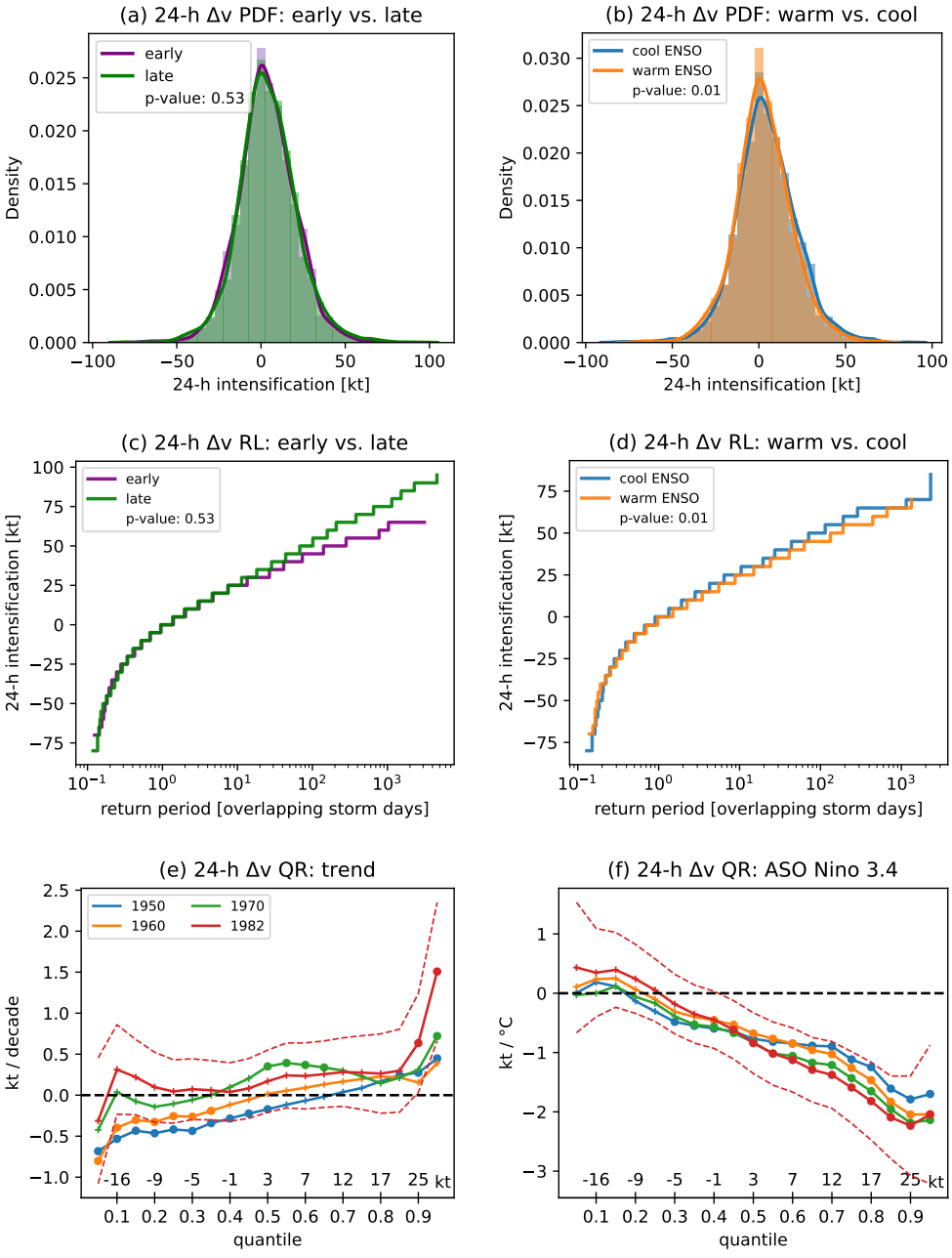

FIG. 5. Histograms and kernel-smoothed probability density functions (PDFs) of Atlantic 24-h intensification (24-h Δv) 1982–2024 during (a) early and late periods and (b) warm and cool ENSO conditions. Return level (RL) curves for Atlantic 24-h intensification (1982–2024) during (c) early and late periods and (d) warm and cool ENSO conditions. Atlantic 24-h intensification quantile regression (QR) coefficients for the (e) trend and (f) Niño-3.4. Colors indicate start year shown in legend. 95% confidence intervals are shown (red dashed lines) for the 1982–2024 coefficients. Filled circles indicate statistically significant (5% level) coefficients. Quantile values are shown for reference in (e) and (f) for the full 1982–2024 data.

trends in the lower quantiles are significant when the analysis start year is 1950 or 1960, but not for later start years (Fig. 5e). Niño-3.4 quantile coefficients are negative and significant above the 0.45 quantile (positive intensification values) and decrease with increasing quantile up to the 0.9 quantile (-2.2 kt $°C^{-1}$; Fig. 5f), consistent with the composite results.

b. Lifetime maximum 24-h intensification

LM24I is a new per storm intensification diagnostic which has not been examined previously for trends or ENSO-related variability. The difference between the distributions of Atlantic LM24I during early and late periods is not significant (Fig. 6a). There is a shift above 30 kt to shorter return periods in the late period, and this shift is largest at the extreme right tail (Fig. 6c). In the early period the largest LM24I value is 65 kt (Andrew, 1992; Keith, 2000) and in the late period it is 95 kt (Wilma, 2005). The difference between the distributions of LM24I intensification in warm and cool ENSO years is significant with a shift to higher values during the cool years (Figs. 6b, d). This shift to higher values during cool ENSO conditions is present across nearly all values and is fairly uniform. The largest LM24I value during a warm ENSO year is 70 kt (Lee, 2023), and during a cool ENSO year it is 85 kt (Felix, 2007). Quantile regression of LM24I with time and Niño-3.4 as covariates show that significant trends are limited to the 0.9 and 0.95 quantiles (3.5 and 4.8 kt $decade^{-1}$; Fig. 6e). Most Niño-3.4 quantile coefficients are significant (Fig. 6f) with values near that of the median coefficient value of -3.3 kt $°C^{-1}$. The largest trend is -5.3 kt $°C^{-1}$ for the 0.95 quantile. Both sets of coefficients are fairly robust with respect to choice of start year with the largest changes tending to be at the highest quantiles.

c. RI event and storm frequency

There are substantially more RI events per year during the late period compared to the early period at all thresholds (not shown). For instance, there are 17.6 RI events per year during the late period and 10.6 per year during the early period for the 30 kt RI threshold, which is an increase of about 66%. However, looking at RI event numbers alone fails to account for the cases when RI did not occur. In fact, there are 152 overlapping 24-h storm periods per year in the early period and 215 overlapping 24-h storm periods per year in the late period. Therefore, an increase in the number of RI events would be expected without a change in RI frequency. The odds ratio is

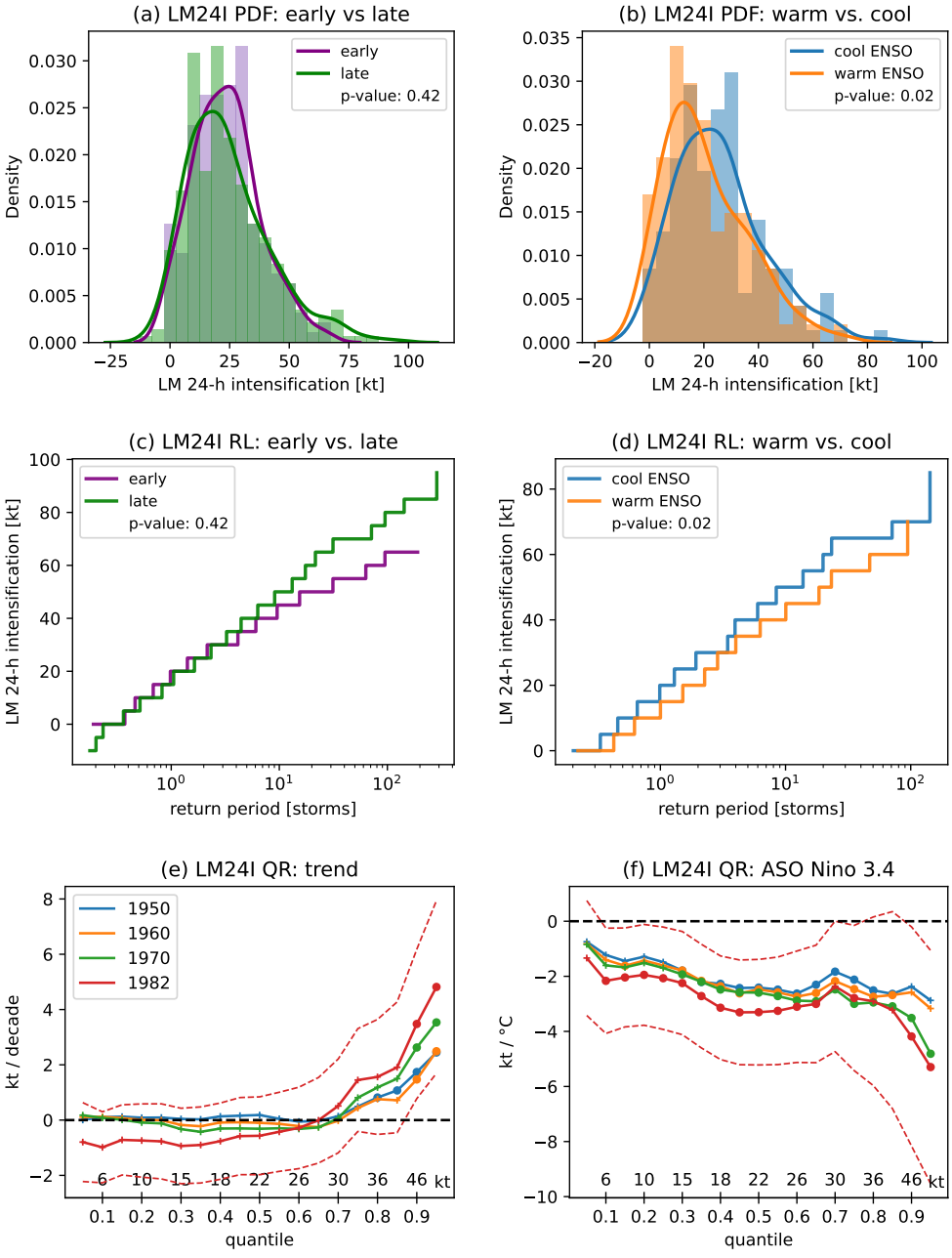

FIG. 6. As in Fig. 5 but for Atlantic lifetime maximum 24-h intensification (LM24I).

the ratio of RI events to non-RI events. The odds ratios between early and late periods indicate significant increases in RI frequency during the late period for thresholds above 25 kt (Fig. 7a). The RI early vs. late odds ratios for thresholds of 20 kt and 25 kt are near one and are statistically insignificant. RI frequency increases at all thresholds during cool ENSO years compared with warm ENSO years, and the increase is statistically significant at thresholds below 35 kt (Fig. 7b).

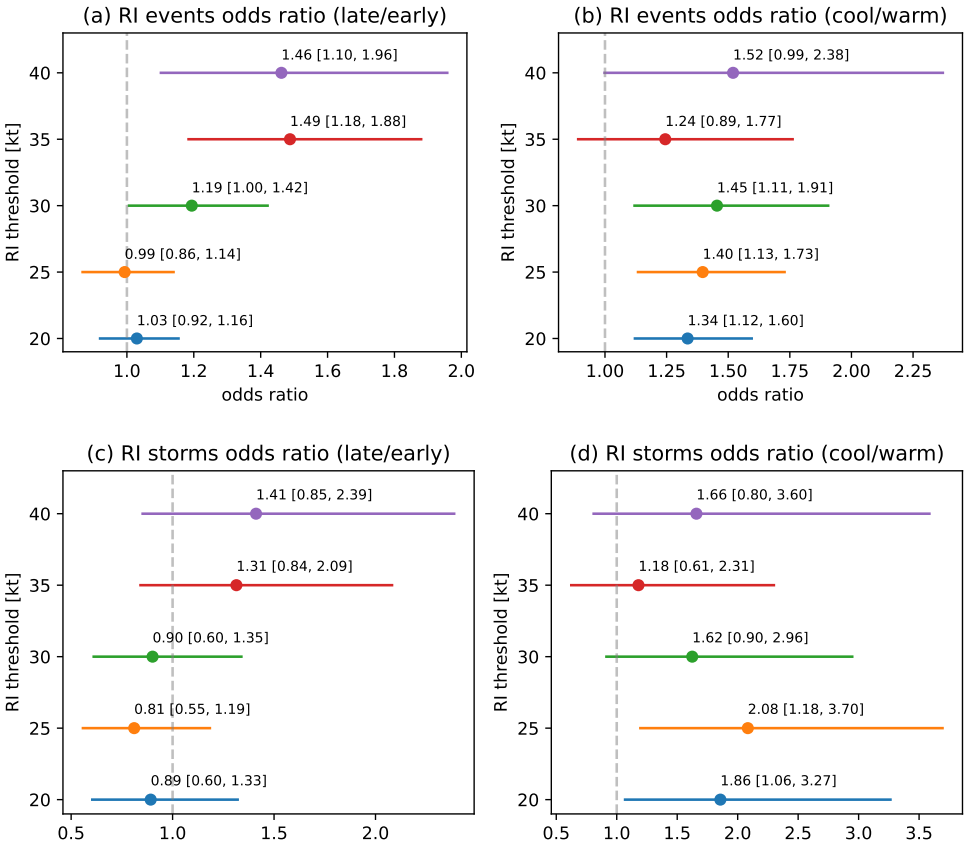

FIG. 7. Odds ratios (dots) with 95% confidence intervals (horizontal lines) for Atlantic RI events during (a) early vs. late periods and (b) warm vs. cool ENSO years, and for Atlantic RI storms (c) early vs. late periods and (d) warm vs. cool ENSO years for RI thresholds of 20 kt to 40 kt by 5 kt.

There are more RI storms per year during the late period than during the early period at all thresholds (not shown). However, there are also more storms overall (RI and non-RI) per year during the late period. The odds ratio indicates that RI storm frequency decreases during the late period for thresholds up to 30 kt and increases for thresholds of 35 kt and 40 kt (Fig. 7c). None of the RI storm frequency changes between the early and late periods are statistically significant. The number of RI storms (not shown) as well as their frequency increase during cool ENSO years compared to warm ENSO years (Fig. 7d). Only the ENSO-related RI storm frequency increases at 20 kt and 25 kt are statistically significant at the 5% level.

Logistic regression shows that decreases in Niño-3.4 are accompanied by increases in the probability of RI events and RI storms for all RI thresholds (olive dots in in Figs. 8a, b). The

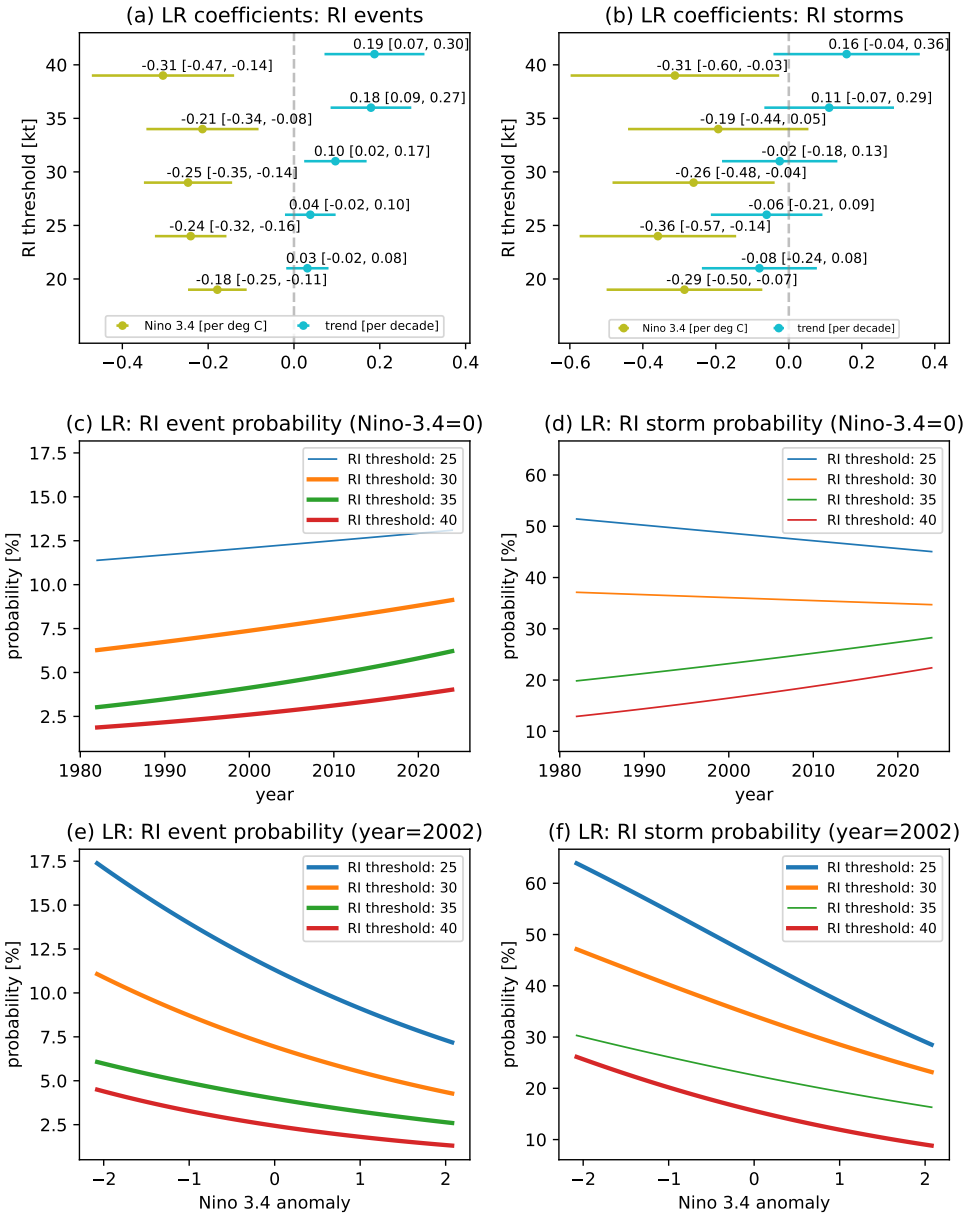

FIG. 8. Logistic regression (LR) coefficients (dots) for time and Niño-3.4 along with their 95% confidence intervals (horizontal lines) for the probability of (a) Atlantic RI events and (b) Atlantic RI storms. Logistic regression-fitted probability of Atlantic RI events as a function of (c) time and (e) Niño-3.4, and probability of Atlantic RI storms as a function of (d) time (f) Niño-3.4. For varying time, Niño-3.4 is fixed to its average value of zero anomaly; for varying Niño-3.4, time is fixed to its average value 2002. Fitted values with thick lines correspond to logistic regression coefficients that are statistically significant at the 5% level.

corresponding logistic regression coefficients are statistically significant (confidence intervals do not include zero) in all cases except RI storm probability with a 35-kt threshold. The probability of RI events has a positive trend for all thresholds, and the corresponding logistic regression coefficients are statistically significant for thresholds of 30 kt and above (cyan dots and lines in Fig. 8a). The finding of a statistically significant trend in RI frequency for threshold of 30 kt improves upon the OLS analysis of annual proportions in Fig. 3 which did not find a significant trend. We return to this point in Section 5. The probability of RI storms decreases with time for thresholds below 35 kt and increases for thresholds of 35 kt and 40 kt, which matches the composite behavior (Fig. 7c). None of the logistic regression trend coefficients for RI storms are statistically significant (confidence intervals include zero; cyan lines in Fig. 8b).

To visualize the trends in the probability of RI events and storms, we set the Niño-3.4 anomaly to zero and varied the year over its observed range 1982–2024 (Figs. 8c, d). For a RI threshold of 30 kt, the event probability increases from 6.3% to 9.1% (0.07 pp decade^{-1}, slightly above the OLS value in Fig. 4c), and the RI storm probability decreases from 37.1% to 34.7% (-0.06 pp decade^{-1}). Likewise, to visualize the dependence of RI event and RI storm probability on Niño-3.4, we set the year to its midpoint value of 2002 and varied Niño-3.4 over its observed range (Figs. 8e, f). For a RI threshold of 30, the event probability varies from from 11.1% to 4.3% (-1.6 pp °C^{-1} Niño-3.4) and the storm probability varies from 47.1% to 23.2% (-5.8 pp °C^{-1} Niño-3.4). The variation in probability of RI events and RI storms over the observed range of Niño-3.4 values is larger than that from trends over the period 1982–2024.

d. Lifetime maximum intensity

Differences between the Atlantic LMI distributions in early and late periods are statistically insignificant (Fig. 9a), though this result is sensitive to the choice of period. The p-value drops to 0.01 when the start year is 1980 (not shown). LMI values above 100 kt are more frequent (shorter return period) in the late period and intensity values in the range of tropical storms are less frequent (longer return period; Fig. 9c). The difference in Atlantic LMI distributions between warm and cool ENSO years is also statistically insignificant (Fig. 9b). For LMI values above 50 kt, there is a consistent shift toward shorter return periods (more frequent occurrence) during cool ENSO years (Fig. 9d). Quantile regression provides a more detailed description of these distributional changes.

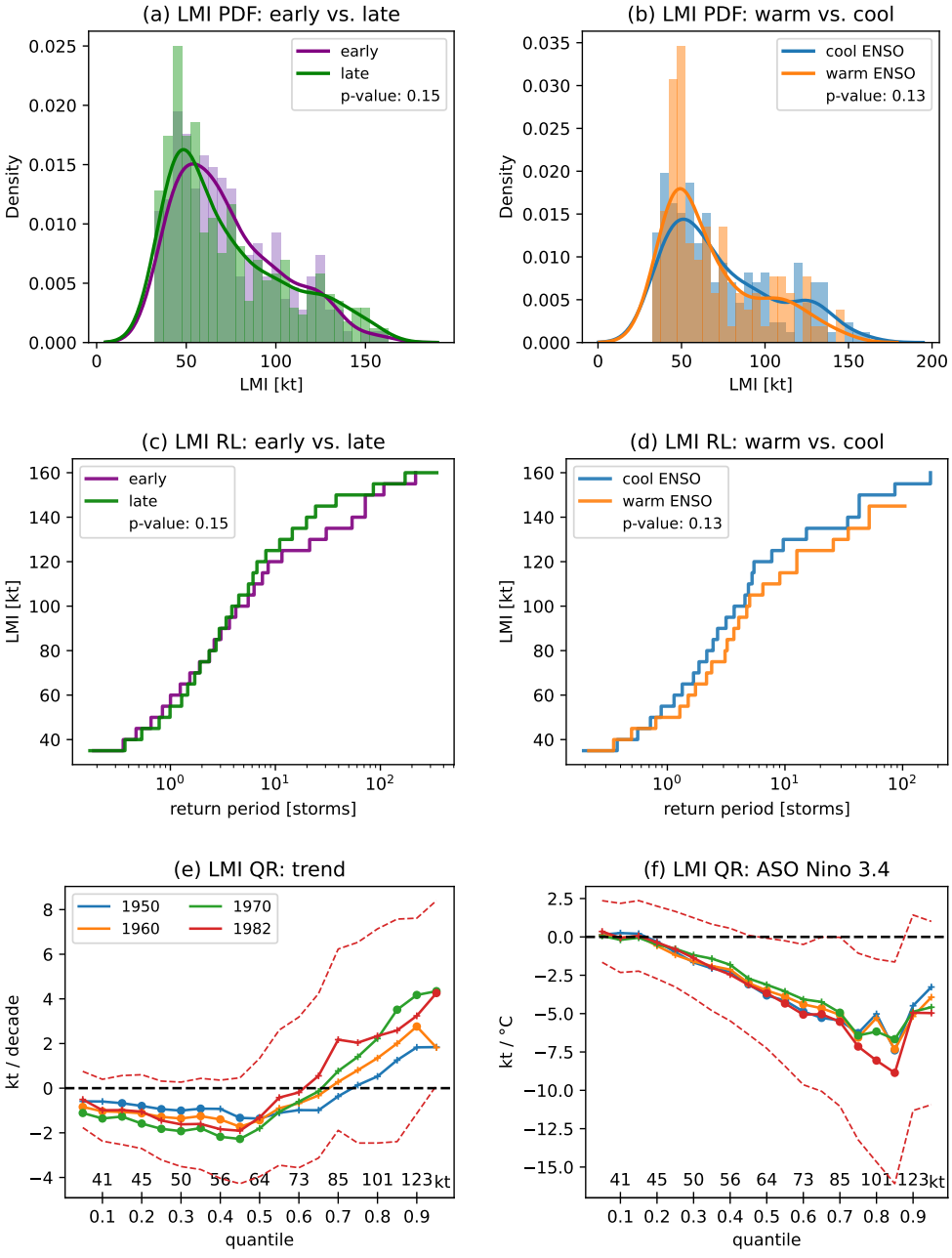

FIG. 9. As in Fig. 5 but for Atlantic lifetime maximum intensity (LMI).

Trends in the 0.05–0.5 quantiles (tropical storm range) are negative and significant for all periods except 1982–2024 (Fig. 9e). The 0.95 quantile trend of 4.3 kt decade^{-1} is significant for the periods 1970–2024 and 1982–2024, though the significance is marginal in the sense that the lower limit of the 5% confidence interval is only slightly above zero. The trend is smaller (3.8 kt decade^{-1}) and not significant if Niño-3.4 is removed from the quantile regression (not shown). Niño-3.4 quantile

coefficients are negative and significant for quantiles in the range 0.45–0.85, which corresponds to Cat 1–3 hurricanes (Fig. 9f). The largest Niño-3.4 coefficient is -8.9 kt $°C^{-1}$ for the 0.85 quantile (110 kt on average).

5. Summary and conclusions

Here we have examined trends and ENSO-related variability in Atlantic tropical cyclone intensities and intensification from IBTrACS data. The quantities considered were: 24-h intensification, lifetime maximum 24-h intensification (LM24I), and lifetime maximum intensity (LMI). We also considered the frequency of rapid intensification (RI; 24-h intensification exceeding thresholds of 20 kt to 40 kt by 5 kt) and the frequency of RI storms (storms that undergo RI during their lifetime). We focused on the period 1982–2024 and characterized the ENSO state by the August–October Niño-3.4 index. We diagnosed trends and ENSO-related variability using composite analysis (simple and straightforward to interpret), quantile regression (for distributional changes), and logistic regression (for frequency changes). Logistic regression for RI is common in forecast applications, but its use here to assess trends and ENSO dependence in the frequency of RI events and RI storms appears to be novel.

Significant trends in 24-h intensification are limited to the 0.9 and 0.95 quantiles with values of 0.6 kt $decade^{-1}$ and 1.5 kt $decade^{-1}$, respectively. Higher trend values previously reported for the period 1982–2009 might be due to unusually low and high values near the start and end of that period, respectively. The modest trends isolated to the highest quantiles may be the reason that composites of early and late period 24-h intensification distributions show no significant difference. A new finding is that the distribution of Atlantic 24-h intensification differs significantly between warm and cool ENSO years. At the quantile level, the 0.4 through 0.95 quantiles of Atlantic 24-h intensification (roughly the positive values) increase significantly with decreasing values of Niño-3.4, about 2 kt $°C^{-1}$ of Niño-3.4 cooling at the higher quantiles. Upward trends in the high quantiles of 24-h intensification would be expected to increase Atlantic RI frequency, and indeed composite analysis and logistic regression show significant increases in Atlantic RI frequency over time for RI thresholds of 30 kt and higher. Similarly, we found significant increases in Atlantic RI frequency with decreasing values of Niño-3.4 at all RI thresholds using logistic regression. The finding that Atlantic RI frequency (not only number of RI events) increases during cool ENSO

conditions extends the work of Klotzbach (2012, their Fig. 2) who found that more RI events occur during La Niña conditions than during El Niño conditions.

Trends in the frequency of Atlantic RI storms are mixed. Trends are negative for RI thresholds up to 30 kt and positive for thresholds of 35 and 40 kt, but none are statistically significant. The ENSO relation with RI storm frequency is negative for all RI thresholds. Composite analysis finds that the increase in RI storm frequency during cool ENSO conditions is statistically significant for RI thresholds of 25 kt and 30 kt, while logistic regression finds they are significant at all RI thresholds except 35 kt. As an alternative to the yes/no threshold-dependent RI storm classification, we introduced a new per storm intensification metric called lifetime maximum 24-h intensification (LM24I). We see LM24I as complementary to RI storm classification (i.e., deciding whether a storm undergoes RI at some point during its lifetime) with the advantage of not depending on a threshold and being a continuous rather than dichotomous quantity. Similar to 24-h intensification, we found significant positive trends in 0.9 and 0.95 quantiles of LM24I, though with larger values, 3–5 kt decade^{-1}, perhaps because LM24I is a maximum over storm lifetime. We found significant changes in the Atlantic LM24I distribution between warm and cool ENSO years, as well as significant increases of 2–5 kt across most quantiles for each °C of Niño-3.4 cooling.

We found negative trends in Atlantic LMI quantiles below the median (tropical storm strength) whose statistical significance varied with period. Positive trends in the 0.95 quantile (4.3 kt decade^{-1}) are significant over the periods 1970–2024 and 1982–2024. The LMI trends that we found here are smaller than the 15.6 kt decade^{-1} (8 m s^{-1} decade^{-1}) that Kossin et al. (2013) found in Atlantic storms with LMI over 65 kt over the period 1982–2009. The difference in LMI trend estimates may reflect sensitivity to period since LMI values for both tropical storms and Category 1+ hurricanes were low around 1982 and show little upward trend after 2009 (Fig. 10). A new finding is that the 0.45 to 0.85 quantiles of Atlantic LMI (roughly Category 1–3 hurricanes) have a significant negative relation with Niño-3.4 that reaches -8.9 kt °C^{-1} for the 0.85 quantile. No LMI trends are significant over the period 1982–2024 when Niño-3.4 is removed from the quantile regression, which supports the argument that accounting for ENSO variability can improve trend estimates.

An important methodological point which seems to have received little attention previously is that statistical analysis of best-track intensity data can be improved by adding jitter (small

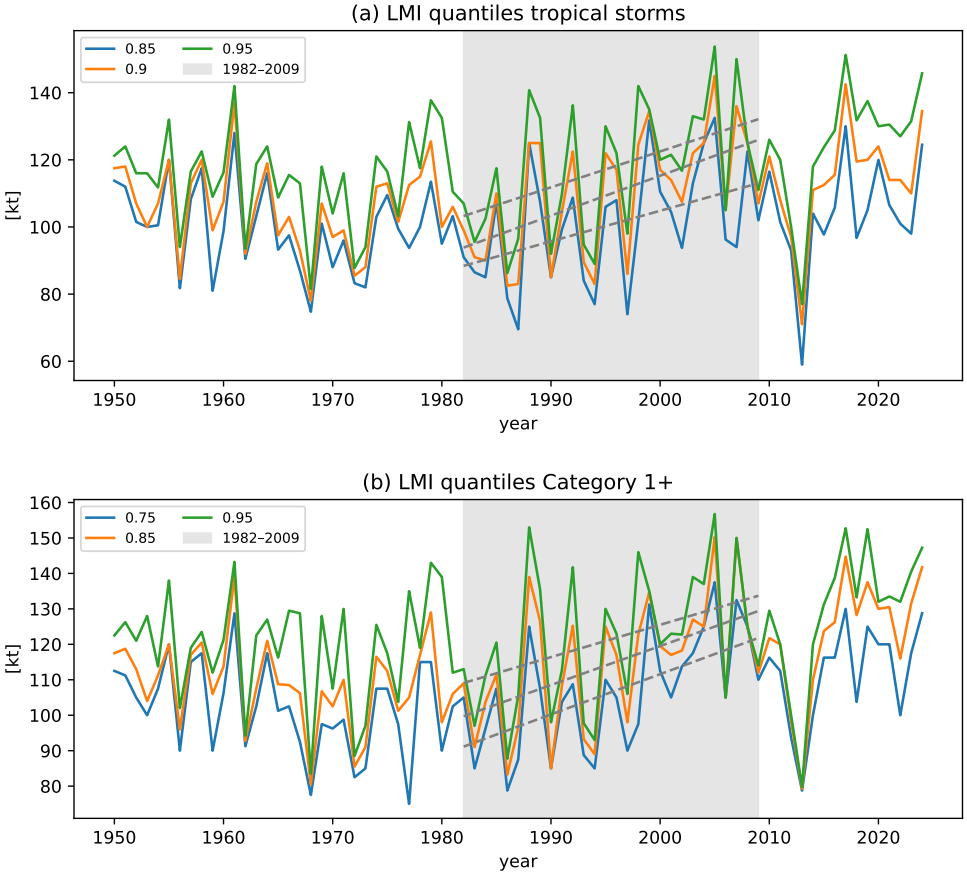

544 FIG. 10. Annual quantiles (probability level in legend) of Atlantic LMI 1950–2024 for (a) tropical storms and
545 (b) storms rated Category 1+. Values during the period 1982–2009 (shaded) are fit to a linear trend by OLS
546 regression and the trend lines are plotted.

549 random numbers). Best-track intensity data are rounded to the nearest 5 kt, which can lead to
550 poor performance of statistical methods that assume continuous distributions. Here we used jitter
551 consisting of random numbers uniformly distributed on the interval ±2.5 kt, which fills in the gaps
552 in the data. Experiments with synthetic data demonstrated that 5 kt rounding increases the error of
553 quantile estimates and that suitable jitter decreases the error. We also showed that without jitter,
554 quantile regression may be unstable and give incorrect confidence intervals. However, the purpose
555 of adding jitter is not to compute uncertainty or statistical significance. We established here that the
556 jitter-based uncertainty quantification procedure of Bhatia et al. (2019) produces biased quantile
557 estimates and overestimates the statistical significance of trends.

Comparing the results here with some prior ones that we repeated here provided an opportunity to compare OLS regression of annual values with logistic and quantile regression. One key difference is that OLS regression of annual values (proportions or quantiles) fails to account for the number of events that go into the calculation of the annual value. As an extreme illustration of this point, consider RI events in 1990 and 1991 when RI occurred in 1 out 205 24-h periods and in 5 out of 54 24-h periods, respectively. An intercept-only regression estimates the average frequency, and logistic regression gives the correct average frequency for these two years as (1 + 5)/(205 + 54) = 2.3%. On the other hand, using annual proportions gives (1/205 + 5/54)/2 = 4.9%, which can be interpreted as giving too much weight to the year 1991 which has relatively few samples. We saw two cases where this difference seemed to impact significance results. First, logistic regression found a significant positive trend in Atlantic RI frequency 1982–2024 but OLS regression of annual proportions did not (compare Figs. 4c and 8a). The trend-only logistic regression is also significant (not shown) which suggests the difference is due to the differing regression methods, not the inclusion of Niño-3.4. We speculate that the varying number of events from year to year might play a role. The years 1991 and 2013 were inactive ones with relatively few RI opportunities, less than 50% of average. However, their annual RI proportions, 29% and 0%, respectively, were in opposition to an upward trend. OLS regression weights these years more than logistic regression does, which might lead to the OLS trend being insignificant. The OLS trend is significant when those two years are removed. Second, the OLS regression of the 0.9 and 0.95 annual quantiles of 24-h intensification found that the 1982–2024 trends were insignificant (Figs. 4a, b), but quantile regression found the trends to be significant (Fig. 5). The same consideration about unequal weighting applies to quantile regression. In this case, the trend-only quantile regression finds the 0.95 quantile trend significant but including Niño-3.4 in the regression is required to obtain the (marginal) significance of the 0.9 quantile.

The findings here suggest several directions for future work. Similar analysis could be applied to global intensity data and to intensity data from other basins. Previous work has found different trends (Balaguru et al. 2018) and ENSO dependence in RI (Klotzbach 2012) in different Atlantic sub-basins. The analysis here could be applied at sub-basin scale. An interesting question is whether models simulate the same trends and ENSO relations as seen in observations. Although models have limitations, especially related to intensity, their deficiencies are distinct from the ones

in best-track data. Model experiments could also address the issue of attributing trends (Murakami 2022). Although ENSO forecast skill is relatively low for August–October targets (e.g., Fig. 10.3 of L'Heureux et al. 2020), ENSO forecasts could potentially be translated into seasonal intensity predictions. Whether such forecasts have skill and how that skill depends on lead time could be tested by repeating the analysis here with observed values of the Niño-3.4 index replaced by forecast ones, analogous to Lepore et al. (2017) or Villarini et al. (2019). We have used the Niño-3.4 index to characterize the ENSO state, but relative Niño-3.4 which removes the tropical mean SST might provide a better measure of ENSO teleconnections in a warming climate (Van Oldenborgh et al. 2021; L'Heureux et al. 2024). El Niño diversity might also play a role in modulating Atlantic tropical cyclone intensities (Patricola et al. 2016). Future work should consider trends and ENSO-related variability in tropical cyclone intensity as measured by surface pressure (Klotzbach et al. 2020).

This study has tried to avoid some of the problems of best-track intensity data by addressing 5 kt discretization, focusing on the period during which satellite data are available, and limiting our attention to a single basin and data-providing agency, but there might be other data issues that could impact the results. For instance, data quality may vary over time, which has not been taken into account here. This issue might impact analysis of trends more directly than analysis of ENSO variability. The Advanced Dvorak Technique Hurricane Satellite (ADT-HURSAT) data record offers a temporally consistent (albeit less accurate) view of tropical cyclone intensity (Kossin et al. 2013, 2020). However, ADT-HURSAT "is not designed to be a substitute for the best track, nor is it designed to be used on a point-by-point or storm-by-storm basis" (Kossin et al. 2020), which has implications for its use in intensification studies. In particular, previous studies have noted that intensification that occurs under dense cirrus cloud may result in ADT intensity values that remain constant and then rapidly increase when the eye appears (Kossin et al. 2013, 2020). Consequently, extreme intensification values are more frequent in ADT-HURSAT data than in IBTrACS (Bhatia et al. 2018, 2019). This behavior is seen in the case of Edouard (2014) where IBTrACS shows gradual intensification (maximum value of 25 kt d^{-1}), and ADT-HURSAT show abrupt intensification (maximum value of 55 kt d^{-1}; Fig. 11a). Over the period 1978–2017, quantiles of positive 24-h intensification (Fig. 11b) and quantiles of LM24I (Fig. 11c) are larger in ADT-HURSAT than in IBTrACS. As a result, the annual frequencies of RI (Fig. 11d) and RI

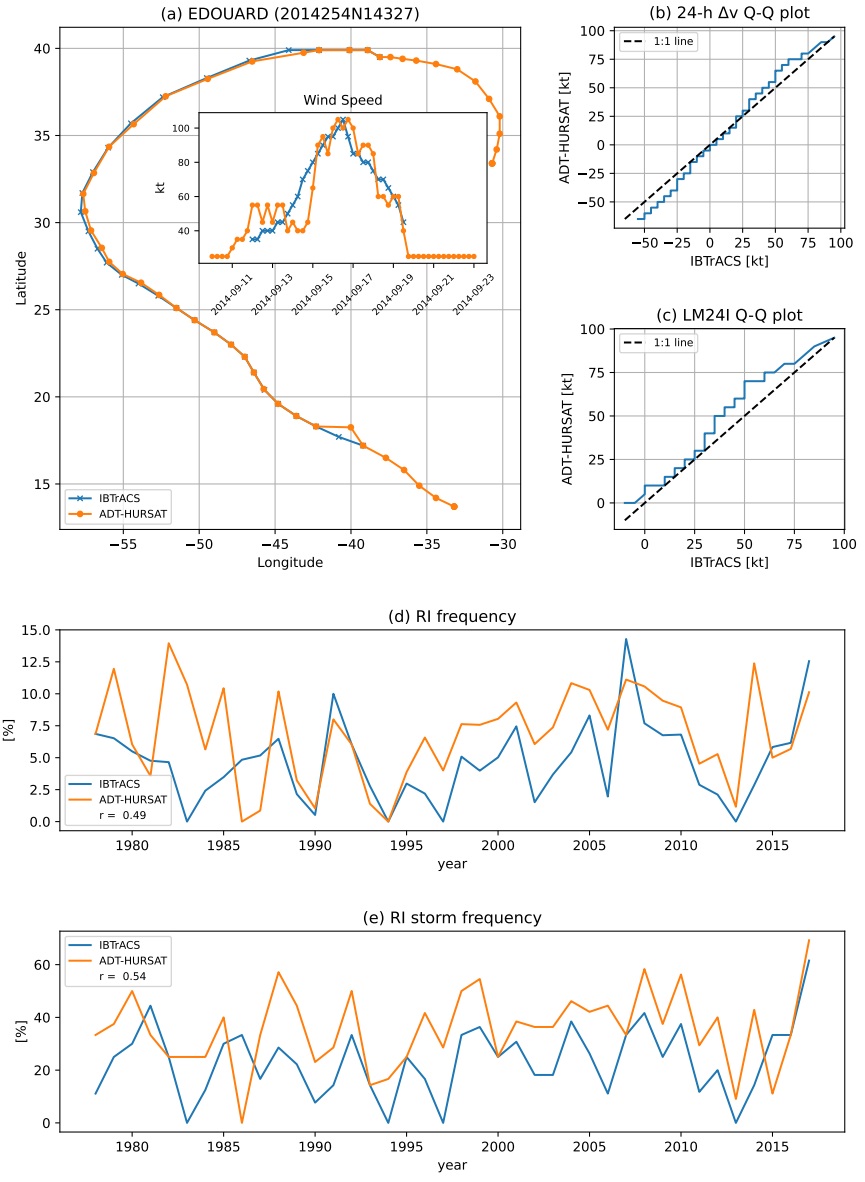

FIG. 11. (a) Track and intensity (inset) of Edouard (2014) in IBTrACS and ADT-HURSAT. Quantile-quantile plots of (b) 24h-intensification and (c) LM24I. Annual frequencies 1978–2017 of (d) RI events and (e) RI storms using a 35 kt threshold in IBTrACS and ADT-HURSAT along with their correlation. Panels (d)–(e) use matching IBTrACS and ADT-HURSAT 24h-intensification data.

storms (Fig. 11e) tend to be larger in ADT-HURSAT than in IBTrACS. The modest correlations between those timeseries in the two datasets further support caution when using ADT-HURSAT on a point-by-point or storm-by-storm basis.

Acknowledgments. SJC acknowledges support from NSF (AGS-2043142, AGS-2217618, and AGS-224491), NOAA (NA21OAR430345, NA22OAR4310610) and DOE (DE-SC0023333). We thank three anonymous reviewers for their useful comments and suggestions.

Data availability statement. North Atlantic International Best Track Archive for Climate Stewardship data was downloaded from `https://www.ncei.noaa.gov/data/international-best-track-archive-for-climate-stewardship-ibtracs/v04r01/access/csv/ibtracs.NA.list.v04r01.csv`. NOAA Extended Reconstructed SST V5 data provided by the NOAA PSL, Boulder, Colorado, USA, from their website at `https://downloads.psl.noaa.gov/Datasets/noaa.ersst.v5/sst.mnmean.nc`. ADT-HURSAT data are taken from the Supporting Information `https://www.pnas.org/doi/10.1073/pnas.1920849117#supplementary-materials` of Kossin et al. (2020).

References

Balaguru, K., G. R. Foltz, and L. R. Leung, 2018: Increasing magnitude of hurricane rapid intensification in the central and eastern tropical Atlantic. *Geophysical Research Letters*, **45**, 4238–4247.

Balaguru, K., G. R. Foltz, L. R. Leung, W. Xu, D. Kim, H. Lopez, and R. West, 2022: Increasing hurricane intensification rate near the US Atlantic coast. *Geophysical Research Letters*, **49**, e2022GL099 793.

Barnston, A. G., M. Chelliah, and S. B. Goldenberg, 1997: Documentation of a highly ENSO-related SST region in the equitorial Pacific. *Atmosphere-Ocean*, **35**, 367–383.

Becker, E. J., and M. K. Tippett, 2024: Impact of ENSO and trends on the distribution of North American wintertime daily temperature. *Journal of Climate*, **37**, 3509–3520, https://doi.org/10.1175/JCLI-D-23-0569.1.

Bhatia, K., G. Vecchi, H. Murakami, S. Underwood, and J. Kossin, 2018: Projected response of tropical cyclone intensity and intensification in a global climate model. *Journal of climate*, **31**, 8281–8303.

Bhatia, K., and Coauthors, 2022: A potential explanation for the global increase in tropical cyclone rapid intensification. *Nature Communications*, **13**, 6626, https://doi.org/10.1038/s41467-022-34321-6.

Bhatia, K. T., G. A. Vecchi, T. R. Knutson, H. Murakami, J. Kossin, K. W. Dixon, and C. E. Whitlock, 2019: Recent increases in tropical cyclone intensification rates. *Nature Communications*, **10**, 1–9.

Bove, M. C., J. B. Elsner, C. W. Landsea, X. Niu, and J. J. O'Brien, 1998: Effect of El Niño on US landfalling hurricanes, revisited. *Bulletin of the American Meteorological Society*, **79**, 2477–2482.

Camargo, S. J., and Coauthors, 2023: An update on the influence of natural climate variability and anthropogenic climate change on tropical cyclones. *Tropical Cyclone Research and Review*, **12**, 216–239.

DelSole, T. M., and M. K. Tippett, 2022: *Statistical Methods for Climate Scientists*. Cambridge University Press, https://doi.org/10.1017/9781108659055.

Elsner, J. B., and T. H. Jagger, 2013: Intensity models. *Hurricane Climatology: A Modern Statistical Guide Using R*, Oxford University Press, https://doi.org/10.1093/oso/9780199827633.003.0012.

Gahtan, J., K. R. Knapp, C. J. Schreck, H. J. Diamond, J. P. Kossin, and M. C. Kruk, 2024: International Best Track Archive for Climate Stewardship (IBTrACS) Project, Version 4r01. NOAA, https://doi.org/10.25921/82ty-9e16.

Goldenberg, S. B., C. W. Landsea, A. M. Mestas-Nuñez, and W. M. Gray, 2001: The recent increase in Atlantic hurricane activity: Causes and implications. *Science*, **293**, 474–479.

Gray, W. M., 1984: Atlantic Seasonal Hurricane Frequency. Part I: El Niño and 30 mb Quasi-Biennial Oscillation Influences. *Monthly Weather Review*, **112**, 1649–1668.

Hanley, D. E., M. A. Bourassa, J. J. O'Brien, S. R. Smith, and E. R. Spade, 2003: A quantitative evaluation of ENSO indices. *Journal of Climate*, **16**, 1249–1258.

Huang, B., and Coauthors, 2017: Extended reconstructed sea surface temperature, version 5 (ERSSTv5): Upgrades, validations, and intercomparisons. *Journal of Climate*, **30**, 8179–8205, https://doi.org/10.1175/JCLI-D-16-0836.1.

Jagger, T. H., and J. B. Elsner, 2009: Modeling tropical cyclone intensity with quantile regression. *International Journal of Climatology: A Journal of the Royal Meteorological Society*, **29**, 1351–1361.

Klotzbach, P. J., 2011: El Niño–Southern Oscillation's impact on Atlantic basin hurricanes and US landfalls. *Journal of Climate*, **24**, 1252–1263.

Klotzbach, P. J., 2012: El Niño-Southern Oscillation, the Madden-Julian Oscillation and Atlantic basin tropical cyclone rapid intensification. *Journal of Geophysical Research: Atmospheres*, **117**, D14 104.

Klotzbach, P. J., M. M. Bell, S. G. Bowen, E. J. Gibney, K. R. Knapp, and C. J. Schreck, 2020: Surface pressure a more skillful predictor of normalized hurricane damage than maximum sustained wind. *Bulletin of the American Meteorological Society*, **101**, E830–E846.

Klotzbach, P. J., K. M. Wood, C. J. Schreck III, S. G. Bowen, C. M. Patricola, and M. M. Bell, 2022: Trends in global tropical cyclone activity: 1990–2021. *Geophysical Research Letters*, **49**, e2021GL095 774.

Knaff, J. A., C. R. Sampson, and K. D. Musgrave, 2018: An operational rapid intensification prediction aid for the western North Pacific. *Weather and Forecasting*, **33**, 799–811.

Knapp, K. R., M. C. Kruk, D. H. Levinson, H. J. Diamond, and C. J. Neumann, 2010: The International Best Track Archive for Climate Stewardship (IBTrACS). *Bulletin of the American Meteorological Society*, **91**, 363–376.

Knutson, T., and Coauthors, 2019: Tropical cyclones and climate change assessment: Part I: Detection and attribution. *Bulletin of the American Meteorological Society*, **100 (10)**, 1987–2007.

Knutson, T., and Coauthors, 2020: Tropical cyclones warming world: An assessment of projections. *Bulletin of the American Meteorological Society*, **101**, 771–774.

Knutson, T. R., and Coauthors, 2010: Tropical cyclones and climate change. *Nature geoscience*, **3**, 157–163.

Koenker, R., and G. Bassett, 1978: Regression quantiles. *Econometrica*, **46**, 33–50.

Kossin, J. P., K. R. Knapp, T. L. Olander, and C. S. Velden, 2020: Global increase in major tropical cyclone exceedance probability over the past four decades. *Proceedings of the National Academy of Sciences*, **117**, 11 975–11 980.

Kossin, J. P., T. L. Olander, and K. R. Knapp, 2013: Trend analysis with a new global record of tropical cyclone intensity. *Journal of Climate*, **26**, 9960–9976.

Lee, C.-Y., M. K. Tippett, A. H. Sobel, and S. J. Camargo, 2016: Rapid intensification and the bimodal distribution of tropical cyclone intensity. *Nature Communications*, **7**, 10 625, https://doi.org/10.1038/ncomms10625.

Lepore, C., M. K. Tippett, and J. T. Allen, 2017: ENSO-based probabilistic forecasts of March–May U.S. tornado and hail activity. *Geophys. Res. Lett.*, **44**, 9093–9101, https://doi.org/10.1002/2017GL074781.

L'Heureux, M. L., and Coauthors, 2024: A relative sea surface temperature index for classifying ENSO events in a changing climate. *Journal of Climate*, **37**, 1197–1211, https://doi.org/10.1175/JCLI-D-23-0406.1.

L'Heureux, M. L., A. Levine, M. Newman, C. Ganter, J.-J. Luo, M. K. Tippett, and T. Stockdale, 2020: ENSO Prediction. *El Niño-Southern Oscillation (ENSO) in a Changing Climate*, M. McPhaden, A. Santoso, and W. Cai, Eds., AGU.

Machado, J., and J. Silva, 2005: Quantiles for counts. *J. Am. Stat. Assoc.*, **100**, 1226–1237.

Murakami, H., 2022: Substantial global influence of anthropogenic aerosols on tropical cyclones over the past 40 years. *Science advances*, **8**, eabn9493.

Patricola, C. M., P. Chang, and R. Saravanan, 2016: Degree of simulated suppression of Atlantic tropical cyclones modulated by flavour of El Niño. *Nature Geoscience*, **9 (2)**, 155–160.

Pearson, E. S., 1950: On questions raised by the combination of tests based on discontinuous distributions. *Biometrika*, **37**, 383–398.

Sobel, A. H., S. J. Camargo, T. M. Hall, C.-Y. Lee, M. K. Tippett, and A. A. Wing, 2016: Human influence on tropical cyclone intensity. *Science*, **353**, 242–246, https://doi.org/10.1126/science.aaf6574.

Tang, B. H., and J. Neelin, 2004: ENSO influence on Atlantic hurricanes via tropospheric warming. *Geophysical Research Letters*, **31**, L24 204, https://doi.org/10.1029/2004GL021072.

Tippett, M. K., C. Lepore, and J. E. Cohen, 2016: More tornadoes in the most extreme U.S. tornado outbreaks. *Science*, **354**, 1419–1423, https://doi.org/10.1126/science.aah7393.

Van Oldenborgh, G. J., H. Hendon, T. Stockdale, M. L'Heureux, E. C. De Perez, R. Singh, and M. Van Aalst, 2021: Defining El Niño indices in a warming climate. *Environmental Research Letters*, **16**, 044 003.

Villarini, G., B. Luitel, G. A. Vecchi, and J. Ghosh, 2019: Multi-model ensemble forecasting of North Atlantic tropical cyclone activity. *Climate Dynamics*, **53**, 7461–7477.

Wang, C., X. Wang, R. H. Weisberg, and M. L. Black, 2017: Variability of tropical cyclone rapid intensification in the North Atlantic and its relationship with climate variations. *Climate Dynamics*, **49**, 3627–3645.

Williams, I. N., and C. M. Patricola, 2018: Diversity of ENSO events unified by convective threshold sea surface temperature: A nonlinear ENSO index. *Geophysical Research Letters*, **45**, 9236–9244.

Zhai, A. R., and J. H. Jiang, 2014: Dependence of US hurricane economic loss on maximum wind speed and storm size. *Environmental Research Letters*, **9**, 064 019.